www.acsnano.org

Molecular Beam Epitaxy of Transition Metal (Ti-, V-, and Cr-) Tellurides: From Monolayer Ditellurides to Multilayer Self-Intercalation Compounds

Kinga Lasek, Paula Mariel Coelho, Krzysztof Zberecki, Yan Xin, Sadhu K. Kolekar, Jingfeng Li, and Matthias Batzill*



Downloaded via UNIV OF SOUTH FLORIDA on April 5, 2021 at 12:21:20 (UTC). See https://pubs.acs.org/sharingguidelines for options on how to legitimately share published articles.

Cite This: ACS Nano 2020, 14, 8473-8484



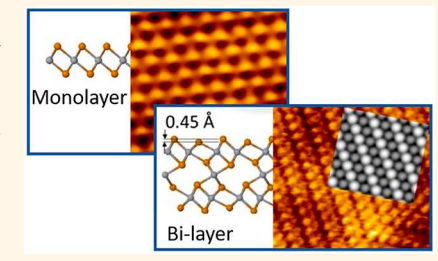
ACCESS

III Metrics & More



Supporting Information

ABSTRACT: Material growth by van der Waals epitaxy has the potential to isolate monolayer (ML) materials and synthesize ultrathin films not easily prepared by exfoliation or other growth methods. Here, the synthesis of the early transition metal (Ti, V, and Cr) tellurides by molecular beam epitaxy (MBE) in the mono- to few-layer regime is investigated. The layered ditellurides of these materials are known for their intriguing quantum- and layer dependent- properties. Here we show by a combination of *in situ* sample characterization and comparison with computational predictions that ML ditellurides with octahedral 1T structure are readily grown, but for multilayers, the transition metal dichalcogenide (TMDC) formation competes with self-intercalated compounds. CrTe₂, a TMDC that is known to be metastable in



bulk and easily decomposes into intercalation compounds, has been synthesized successfully in the ML regime at low growth temperatures. At elevated growth temperatures or for multilayers, only the intercalation compound, equivalent to a bulk Cr₃Te₄, could be obtained. ML VTe₂ is more stable and can be synthesized at higher growth temperatures in the ML regime, but multilayers also convert to a bulk-equivalent V₃Te₄ compound. TiTe₂ is the most stable of the TMDCs studied; nevertheless, a detailed analysis of multilayers also indicates the presence of intercalated metals. Computation suggests that the intercalation-induced distortion of the TMDC-layers is much reduced in Ti-telluride compared to V-, and Cr-telluride. This makes the identification of intercalated materials by scanning tunneling microscopy more challenging for Ti-telluride. The identification of self-intercalation compounds in MBE grown multilayer chalcogenides may explain observed lattice distortions in previously reported MBE grown early transition metal chalcogenides. On the other hand, these intercalation compounds in their ultrathin limit can be considered van der Waals materials in their own right. This class of materials is only accessible by direct growth methods but may be used as "building blocks" in MBE-grown van der Waals heterostructures. Controlling their growth is an important step for understanding and studying the properties of these materials.

KEYWORDS: transition metal dichalcogenides, tellurides, 2D materials, intercalation compounds, molecular beam epitaxy (MBE), thin films, scanning tunneling microscopy

he early transition metal (Ti, V, Cr) dichalcogenides have been studied extensively for their many-body and electron correlation effects, including charge density wave (CDW)-¹⁻⁶ superconductivity⁷⁻¹⁰ transitions, or ferromagnetic ordering. To utilize these materials in advanced van der Waals heterostructures and exploiting proximity effects to tune materials properties, recent work focused on the synthesis of these materials in the mono- to few-layer regime. These early transition metal chalcogenides are chemically sensitive to the environment, challenging the ability to obtain monolayers (MLs) of these materials by mechanical exfoliation or chemical vapor transport growth. The ultraclean environment ensured in

molecular beam epitaxy (MBE) has thus been the most promising approach for the direct growth of these materials. Growth on van der Waals substrates, such as graphene, HOPG, or MoS₂, has demonstrated that many of these materials grow in a van der Waals epitaxy mode, *i.e.*, they maintain the lattice

Received: March 31, 2020 Accepted: June 25, 2020 Published: June 25, 2020





constant of the bulk but align their in-plane crystallographic orientation with that of the substrate. This enables the growth of single-crystalline films on single-crystal substrates.

The early transition metal dichalcogenides (TMDCs) usually exhibit an octahedral coordination of the metals to the chalcogen atoms, known as the 1T structure. This is also the case for the first-row transition metal ditellurides studied here. In addition, VTe2 undergoes a structural transition below ~480 K to a distorted 1T structure, known as the 1T" or ribbon structure, which recently was considered to be associated with a CDW transition for these bulk materials.²⁸ In variance of these known bulk structures, work of MBE grown multilayer structures have indicated structural variations in scanning tunneling microscopy (STM) studies of TiTe₂² VSe₂, 30,31 and VTe₂. 32 These have been interpreted as a transition into a distorted 1T-structure, known as the 1T' structure^{30–32} or the occurrence of periodic lattice distortions in a CDW.²⁹ Such interpretations are controversial, though, because these structures are not known for the bulk of these compounds and explanations for their formation in thin film form, such as interface-induced strain,²⁹ is surprising because of the usually low strain in van der Waals epitaxy. Here we show that similar distortion of the TMDC layer is obtained by self-intercalation of the transition metal in the van der Waals gap, thus providing an alternative explanation for these apparent structural variants in MBE grown multilayers. The formation of such self-intercalation compounds in MBE growth is not surprising because a compositional control of chalcogenides is generally challenging due to the high chalcogen vapor pressure, and the compositional phase diagrams of these early TMDCs contain various intercalation compounds with some of these phases exhibiting lower formation energies than the dichalcogenides.

Here we investigate the challenges and opportunities for synthesizing the early transition metal telluride van der Waals systems by MBE. In a combined experiment and computational study, we show that multilayers prefer growing with self-intercalated transition metals. In contrast, ML TMDCs can be obtained under the right growth conditions, and we show that even for known metastable compounds like CrTe₂, TMDC MLs can be grown by MBE. This understanding of the formation and properties of MBE grown van der Waals materials is a crucial step toward the controlled synthesis of van der Waals heterostructures.

RESULTS AND DISCUSSIONS

An inspection of the compositional phase diagrams of the early-transition metal tellurides shows the existence of several structurally closely related compositions. These compounds may be characterized as a NiAs-like crystal structure with periodic metal vacancies in every second layer. More instructively, they can also be described as an ordered arrangement of metal atoms intercalated in the van der Waals gap of layered TMDCs. ^{33,34} Figure 1 illustrates how the various compositions are related to the basic TMDC structure and only differ by the amount of transition metals in between the TMDC layers. Defining the density of transition metals in the TMDC layer to 1 ML, then compounds with a 1/4, 1/3, or 1/2 ML intercalated transition metals in between the TMDC layers are commonly observed intercalation compounds. Depending on the composition, the intercalated atoms are arranged in a 2 \times 2, ($\sqrt{3} \times \sqrt{3}$)R30°, or 2 \times 1 superstructure, relative to a 1 × 1 unit cell of the TMDC. Clearly, in order to

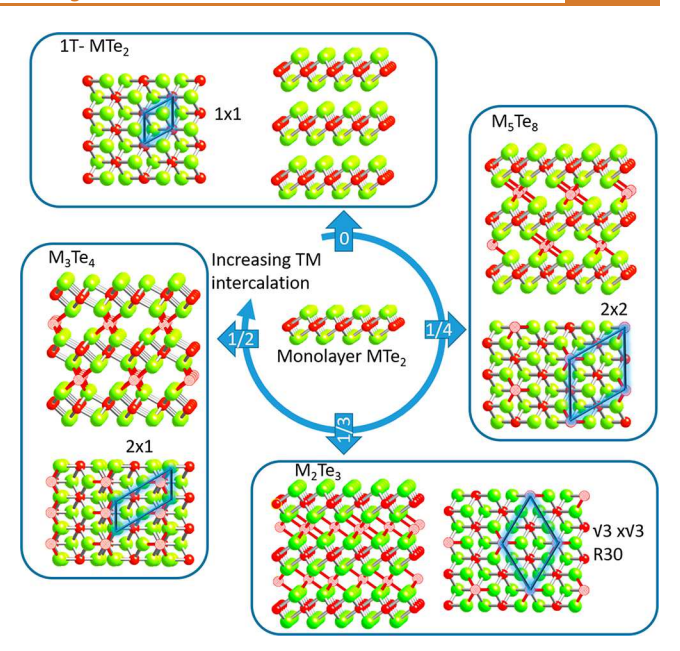


Figure 1. Schematic representation of the relationship between TMDC ML (center) and different bulk compounds. The stacking of TMDC layers results in a bulk MTe $_2$ crystal, while additional M atoms between TMDC layers (indicated as hatched circles) results in various "self-intercalation" compounds. Bulk-compounds with 1/4, 1/3, or 1/2 of extra M atoms are known. The cross-sectional and top views are shown, together with an indication of the supercell of the arrangement of the intercalated atoms with respect to the 1 \times 1 unit cell of the TMDC layer.

form any of these intercalation compounds, two TMDC layers are needed to sandwich the "extra" transition metals. Thus, if one succeeds in reducing the growth to a single layer, one may obtain TMDCs while for multilayers, the formation of TMDCs may compete with the formation of these intercalation compounds.

To assess the stability of the different phases, we conducted total energy DFT calculations. Table 1 shows values of the

Table 1. Computed Values of the Total Energy Per Atom of the Composites Shown in Figure 1 for Bilayer Configurations

| | $\begin{array}{c} {\rm Ti}_{2+x}{\rm Te}_4 \\ {\rm [eV/atom]} \end{array}$ | $\begin{array}{c} V_{2+x}Te_4 \\ [eV/atom] \end{array}$ | $Cr_{2+x}Te_4$ [eV/atom] |
|------------------------|--|---|--------------------------|
| monolayer TMDC $x = 0$ | -5.43 | -5.44 | -5.47 |
| x = 1/4 | -5.57 | -5.60 | -5.67 |
| x = 1/3 | -5.61 | -5.63 | -5.72 |
| x = 1/2 | -5.68 | -5.75 | -5.83 |

total energy per atom for ML TMDCs, as well as bilayers with different amount of intercalated transition metals. Generally, for the intercalation compounds, the material with 1/2 a ML of extra metals is the energetically most favored structure.

Experimentally, it has been shown that ML ditellurides can be obtained by MBE growth for ${\rm TiTe_2}^{17}$ and ${\rm VTe_2}^{.23-27}$ Here, these MLs are the starting point to investigate few-layer films of ${\rm V_xTe_y}$ ${\rm Ti_xTe_y}$. In addition, we study ${\rm Cr_xTe_y}$ from monoto multilayer. In the following, we address these three early TMDCs separately but conclude that they behave similarly. We start our discussion with chromium telluride, the only system in our list that does not have a thermodynamically

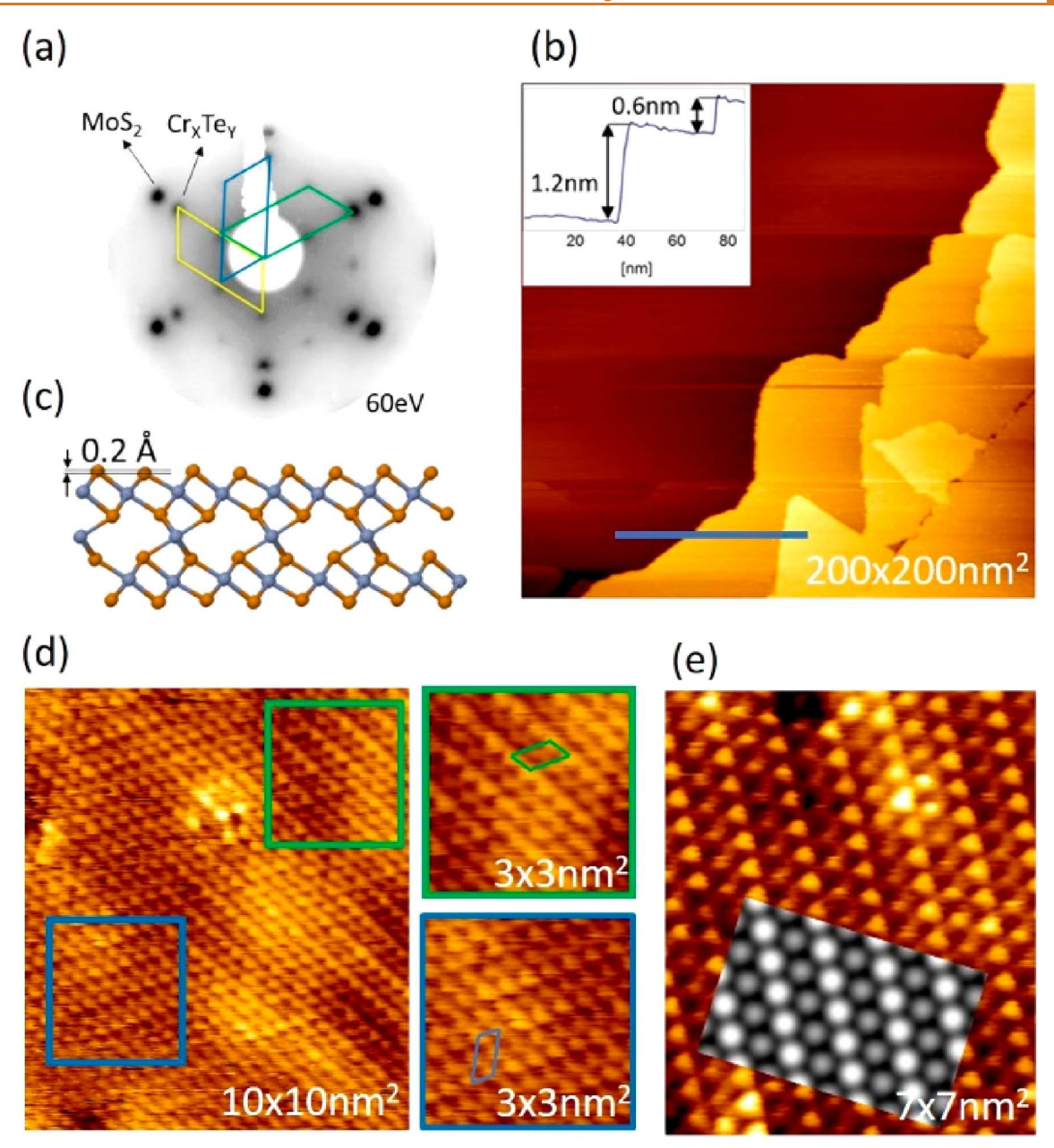


Figure 2. LEED and STM characterization of MBE grown ultrathin Cr-telluride at growth temperature of ~350 °C. (a) LEED of bilayer Cr_xTe_y on MoS_2 substrate, (b) Large scale STM and line profile of a partially covered HOPG substrate. The line profile indicates a bilayer height step of 1.2 nm for the first layer. (c) Side view of the DFT calculated crystal structure of a bilayer $CrTe_2$ with $^1/_2$ layer of Cr intercalation. (d) High-resolution STM of the bilayer regions with two rotational domains. (e) High-resolution STM showing 2 × 1 structure with overlaid simulated STM image for the structure shown in (c). STM imaging conditions (sample bias, tunneling current): (b) 1.4 V, 0.9 nA; (d) 1.4 V, 0.9 nA; (e) 0.1 V, 0.7 nA.

stable MX₂ composition. Chromium telluride is known to form intercalation compounds with a preferred Cr₃Te₄ or Cr₂Te₃ composition,³⁵ and thus an intercalation compound is anticipated for multilayer films, but we will also show that one can reduce the growth to a ML and obtain CrTe₂ in this ultrathin limit. After we have discussed chromium telluride, we show that vanadium telluride behaves very similarly to chromium telluride while for titanium telluride a distinction between TMDCs and intercalation compounds by STM is more challenging.

Chromium Telluride. Chromium tellurides have recently attracted some interests due to their ferromagnetic properties. ^{36–39} The layered-TMDC, CrTe₂, is metastable and can

only be synthesized as a bulk material by first growing a potassium intercalation compound, KCrTe₂, and subsequently chemically extracting the potassium layer. Annealing of such formed CrTe₂ decomposes into Cr₂Te₃ at 330 K, similarly to, but at even lower temperatures, the reported decomposition of CrSe₂ into Cr₂Se₃ and Se at 600 K. Previous reports of MBE growth of chromium telluride also always resulted in either Cr₃Te₄ or Cr₂Te₃. Thus, MBE grown multilayer films are expected to form an intercalation compound, and this may be a good starting point for understanding STM investigations of such intercalation materials.

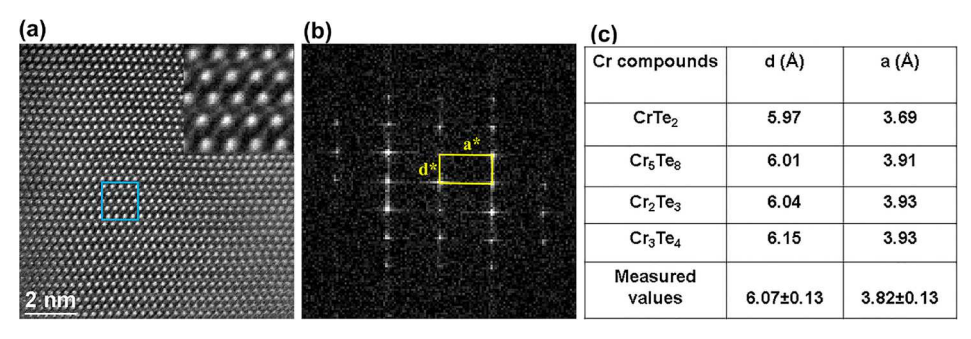


Figure 3. Cross-section HAADF-STEM image of Cr_xTe_y (inset is magnified from the blue box) (a) and respective FFT pattern (b). d* and a* represent the reciprocal vectors of the intercalated compound. (c) Table of lattice constant values for different compounds versus experimental values from TEM measurements (please see Supporting Information for a description of uncertainties).

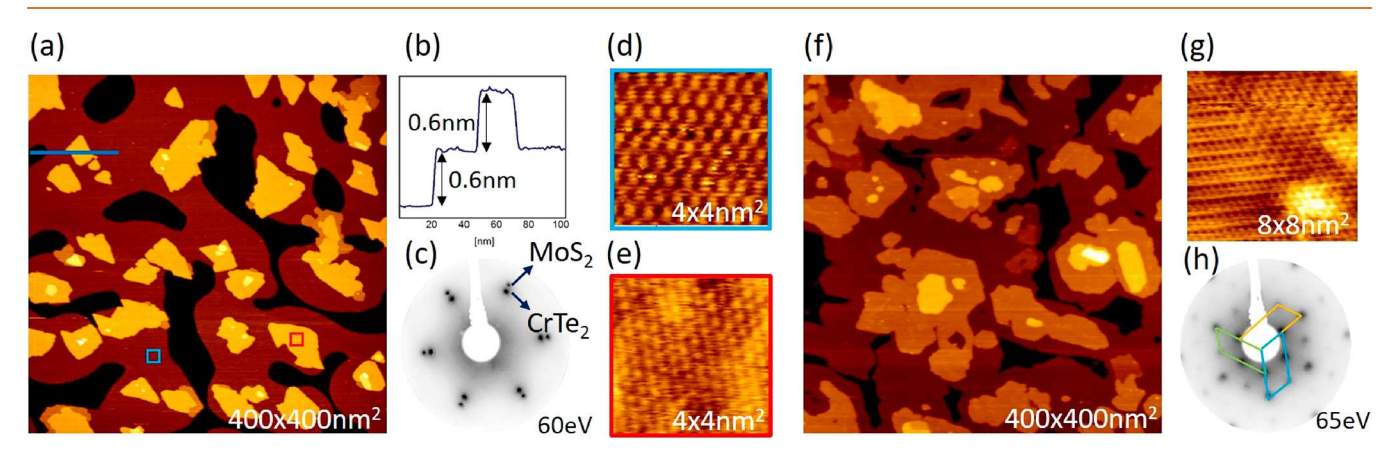


Figure 4. Cr_xTe_y grown at low temperature (200 °C) on MoS_2 substrate. (a) Large scale STM showing a step height of ~0.6 nm for the first layer (b), indicative of ML height. (c) LEED pattern, showing a hexagonal pattern for the ML sample and rotational alignment with the MoS_2 substrate. Atomic resolution STM image of (d) ML and (e) bilayer showing hexagonal pattern with the bilayer presenting an additional height modulation without any long-range periodicity. (f) Large scale STM of multilayer sample. (g) Atomic resolution STM image of multilayer shows 2 × 1 reconstruction. (h) LEED pattern of multilayer films showing a 2 × 1 superstructure. STM imaging conditions (sample bias, tunneling current): (a) 1.3 V, 0.9 nA; (d) -10 mV, 0.8 nA; (e) -5 mV, 1.1 nA; (f) 1.3 V, 0.9 nA; (g) -5 mV, 0.9 nA.

Previous studies of MBE grown chromium telluride were mostly thicker films (~100 nm) and characterized by XRD and/or TEM. A previous STM study of MBE grown Crtelluride only showed large-scale terrace structures without detailed atomic-scale information. 41 Here we grow Cr-telluride on van der Waals substrates, either HOPG or MoS₂, at a growth temperature of 350 °C. On MoS₂, we obtain excellent epitaxial growth (van der Waals epitaxy) and LEED characterization, shown in Figure 2a, shows a 2 × 2 structure with respect to a hexagonal lattice, consistent with either Cr₅Te₈ or Cr_3Te_4 crystal structure (see Figure 1) because a 2 \times 2 hexagonal LEED pattern cannot distinguish between a true 2 × 2 structure or the superpositioning of three rotational 2×1 domains. For few-layer films, diffraction spots from the MoS₂ substrate are also still visible, indicating the crystallographic alignment of the chromium telluride film with the substrate. Large-scale STM images for ultrathin films on either MoS₂ or HOPG substrates, shown in Figure 2b, still exhibit areas that expose the substrate (HOPG in the case Figure 2b). Line profiles indicate that the first terrace has a height of ~1.2 nm and subsequent terraces increase in steps of ~0.6 nm. This suggests that at this growth temperature, chromium telluride does not grow as a single layer TMDC, i.e., CrTe2, but the first layer that forms is already an intercalated bilayer, i.e., two TMDC layers with a layer of Cr intercalated (as illustrated in Figure 2c). Only subsequent terrace steps are the height of an additional TMDC layer (with an intercalated Cr-layer), i.e.,

steps of \sim 0.6 nm. The fact that the first terrace is already an intercalation system is demonstrated by high-resolution STM, shown in Figure 2d. The STM image clearly resolves a 2 \times 1 structure and not a simple hexagonal structure as would be the case for a 1T-CrTe $_2$ layer. The same 2 \times 1 structure is observed for all subsequent layers up to the thickest films grown in this study of about 10 layers. As expected, we also observe rotational domains of the 2 \times 1 structure in the STM images.

While the symmetry of the STM images agrees with an extra $^{1}/_{2}$ ML of metals intercalated, *i.e.*, $\mathrm{Cr_{3}Te_{4}}$ structure, we also performed DFT calculations of the structure and simulated its STM images to confirm the agreement between STM images and composition. Figure 2c shows the relaxed structure for a bilayer with $^{1}/_{2}$ ML of extra Cr atoms in the gap. The intercalated atoms cause a buckling of the TMDC layer of about 0.2 Å. This topographic corrugation of the surface is also likely to cause the 2 \times 1 contrast in STM. A simulated STM image, using the Tersoff—Hamann approach, 46 overlaid with an experimental image, is shown in Figure 2e and shows good agreement between experiment and calculation. Simulations of other possible intercalation compounds can be found in Supporting Information, Figure S1.

For chromium tellurides the intercalation compounds are also reported⁴⁷ to exhibit larger interlayer separations d, and in-plane lattice constants a, as summarized in the table in

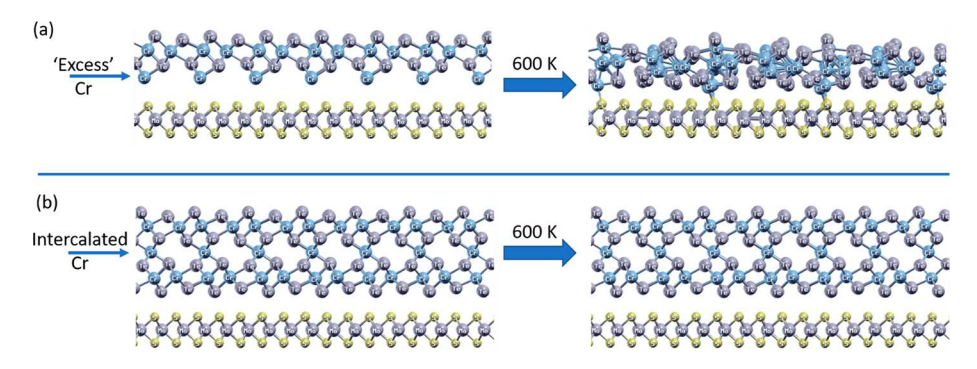


Figure 5. Ab initio molecular dynamics simulations of the stability $CrTe_2$ -films with excess Cr atoms during annealing, (a) ML $CrTe_2$ with $^1/_2$ ML excess Cr in between the ML and a MoS_2 substrate. This structure is not stable and disintegrates with annealing forming an "amorphous" layer. (b) Bilayer $CrTe_2$ with $^1/_2$ ML Cr intercalated in between the two layers. This structure is stable with annealing. Movies of the annealing process are available in the Supporting Information.

Figure 3, compared to 1T-CrTe₂. To evaluate these lattice parameters, cross-sectional high angle annular scanning transmission electron microscopy (HAADF-STEM) studies of multilayer films are conducted and shown in Figure 3. The FFT pattern in part b represent the reciprocal unit cell vectors d* and a* of the STEM image. The FFT is used to determine the real space unit vectors d and a, which are given in Figure 3c as measured values together with lattice parameters ⁴⁶ of known compounds. These measurements further support that the multilayer is an intercalation material and not a TMDC. However, the small differences between the lattice constants of the various intercalation compounds and similar atomic structures projected along this direction do not allow a conclusive determination of the composition of the intercalants.

We have shown that Cr telluride grown at or above 350 °C on either HOPG or MoS2 substrates nucleates and grows as a bilayer with ¹/₂ a ML of metals intercalated. Synthesis of ML CrTe₂ as a potential 2D ferromagnetic TMDC would be highly desirable, though. Therefore, we investigated if ML materials could be stabilized by reducing the growth temperature to 180-250 °C. Indeed, for these reduced growth temperatures, STM reveals the formation of islands with only ~0.6 nm step height indicative of MLs, shown in Figure 4a,b. Such monolayer films can be grown on both HOPG and MoS₂ substrates at these reduced growth temperatures. Moreover, compared to the bilayers formed at higher growth temperatures, the step edges of the ML are meandering without any clear preferred crystallographic orientation. This may be related to the isotropic hexagonal structure of 1T-TMDs compared to the anisotropic structure in intercalated bilayers where the intercalants link two layers and define specific crystallographic directions. LEED for such MLs grown on single crystal MoS₂ substrates (see Figure 4c) also only shows a simple hexagonal pattern. Using the diffraction spots from the substrate and the known lattice constant of MoS_2 (a =0.315 nm) as a calibration, we determine the lattice constant of the ML film to a = 0.36 nm, which is slightly smaller than the lattice constant a = 0.39 nm determined for the bilayer and multilayer films from LEED patterns shown in Figure 2a. Thus, the step height, simple hexagonal pattern, and the lattice constant agrees with CrTe2. Atomic resolution STM images of the terraces of the first layer, shown in Figure 4d, corroborate the simple hexagonal pattern. Atomic resolution images of second layer islands show additional height modulations, however, without any long-range periodicity, see Figure 4e. We

tentatively assign these modulations to disordered intercalated atoms. The growth of multilayer films, shown in Figure 4f, even at these lower growth temperatures, again results in a 2 × 1 superstructure both in STM and LEED (see Figure 4g,h, respectively) and thus is assigned to the same intercalation compound as for the films grown at elevated temperatures. Consequently, 1T-CrTe₂ appears to be only grown successfully as MLs and multilayers convert into intercalation compounds. Nevertheless, the successful growth of ML CrTe₂ will enable their magnetic characterization in future studies.

To demonstrate that the lower growth temperatures are required to obtain MLs, we conducted postgrowth annealing experiments of low temperature grown ML. Annealing of the ML in vacuum to just 300 °C for 30 min converts the predominantly ML sample into a predominantly bilayer sample (see Supporting Information, Figure S2). Moreover, LEED shows a change of the lattice constant from 0.36 nm for the ML to 0.38 for bilayer, consistent with a transition to an intercalation compound. This clearly indicates that the ML is not stable at elevated temperatures and the film is mobile enough to massively rearrange. This also suggests that growth at elevated temperatures will always result in the preferred bilayer structure. The stabilization of the ML at low growth temperature is likely a consequence of the growth kinetics, i.e., the diffusion of adatoms to the growth front of the monolayer. To demonstrate that the ML is CrTe2 and does not have excess Cr in the van der Waals gap between the substrate and the CrTe2-ML, we conducted ab initio molecular dynamics (AIMD) simulations for such structure on a MoS₂ substrate. The results for an "annealing" at 600 K are shown in Figure 5a (similar simulations for excess Cr on top of the CrTe₂ layer can be found in Supporting Information, Figure S3a). In either case with initially $\frac{1}{2}$ ML of excess Cr on-top or below the CrTe₂ layer, the structure is not stable and annealing results in an amorphous film. This contrasts with bilayer $CrTe_2$ with $\frac{1}{2}$ ML of Cr in between the two layers (intercalation compound), shown in Figure 5b, that remains stable. These AIMD simulations thus illustrate that if the ML can be stabilized it will form CrTe₂, and excess Cr are not stable in this structure. In an actual growth scenario, "excess" Cr are thus likely incorporated at the growth front of the CrTe2 ML island. For bilayers, Cr in between two CrTe2 layers are stable and are in fact a lower energy structure than just CrTe2 layers, as our total energy calculations (Table 1) have shown. We further studied the effect of excess Cr "deposited" on top of a bilayer CrTe2 (Supporting Information, Figure S3b). Upon annealing, such

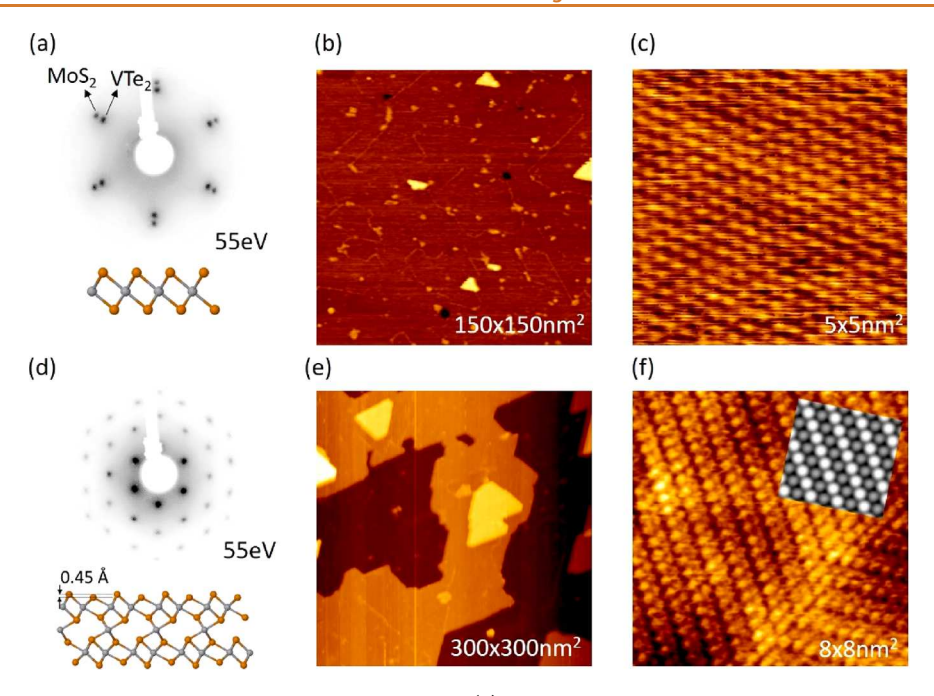


Figure 6. VTe₂ mono- and multilayer films grown on MoS₂ substrate: (a) LEED pattern of ML shows a 1×1 pattern, indicative of epitaxial growth of the film with a 1T structure. (b) Large scale STM image showing that the ML covers the surface uniformly. High resolution STM shown in (c) resolves a simple hexagonal structure. Bi- and multilayer samples grown on MoS₂ substrates exhibit a 2×2 LEED pattern as shown in (d), indicative of three domains of a 2×1 reconstruction. DFT calculations of a bilayer VTe₂ with $^{1}/_{2}$ layer of V intercalated is also shown in (d). The intercalation causes a large buckling of the Te-atoms in the TMDC layer with a corrugation of 0.45 Å. Large scale and high resolution STM images are shown in (e) and (f), respectively. A simulated STM image of the structure in (d) is superimposed on the experimental data in (f). STM imaging conditions (sample bias, tunneling current): (b) 1.2 V, 0.7 nA; (c) 0.2 V, 1.3 nA; (e) 1.2 V, 0.7 nA; (f) -0.1 V, 2 nA.

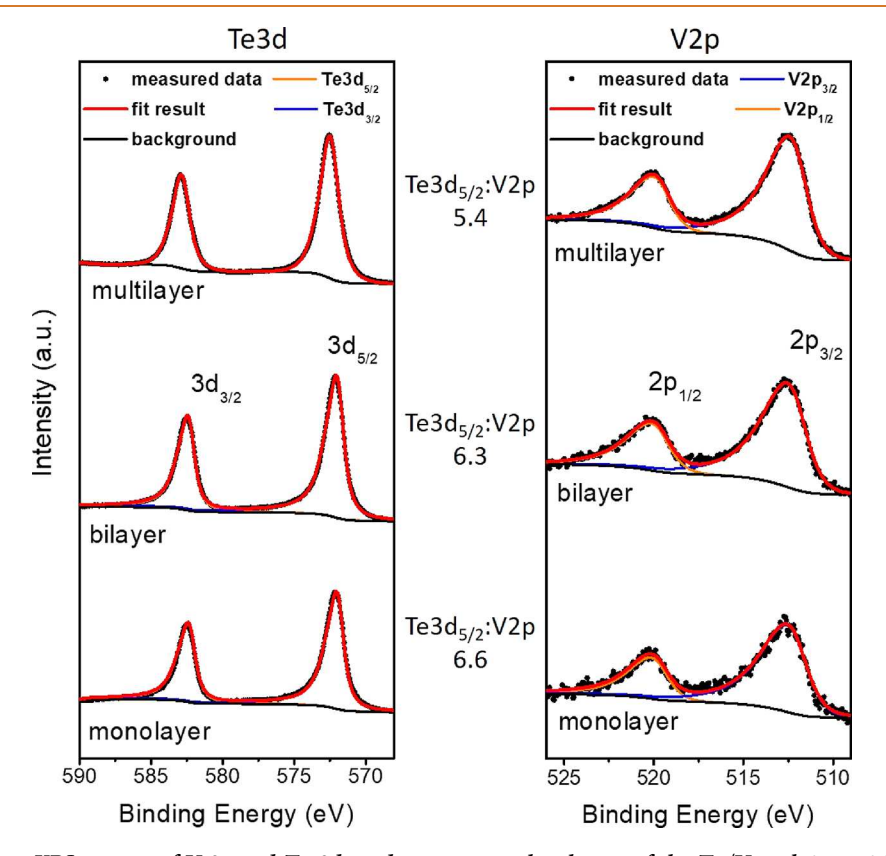


Figure 7. Layer-dependent XPS spectra of V 2p and Te 3d used to compare the change of the Te/V peak intensities as a function of film thickness for V_x Te_y on HOPG samples.

excess atoms get trapped in between the CrTe₂ layers in a process that will lead to an intercalation compound. This indicated that during MBE growth Cr that is provided during the deposition process can be easily incorporated in between two CrTe₂ layers, leading to an intercalation compound. It should be mentioned that during an actual growth, there exist other diffusion pathways for "excess" Cr to get into the gap of two CrTe₂ layers, *e.g.*, from the edges of the growing film. In summary, AIMD simulations verify that CrTe₂ is formed as ML, while in bi- and multilayers Cr easily intercalates in between CrTe₂ layers.

CrTe₂ is known to be metastable in bulk, and thus the easy formation of intercalation compounds in MBE agrees well with this experience from bulk materials. Our total energy calculations (Table 1) for different compounds suggest that Ti- and V-telluride may behave similarly to Cr-telluride, and this is explored in the next two subsections.

Vanadium Telluride. In the bulk, VTe₂ adopts a distorted 1T structure below 480 K, known as the $1T^{\prime\prime}$ structure, ⁴⁸ similar to other group-VB ditellurides. ^{49–51} However, it was shown that MBE grown VTe₂-MLs exhibits the undistorted 1T structure. Moreover, this structure undergoes a 4 × 4 CDW transition at low temperatures. ^{25–27,32} In contrast to CrTe₂, the ML VTe₂ can be obtained even at higher growth temperatures, and an initial nucleation as bilayer films has not been reported for VTe₂. Importantly, we found that bi- and multilayers of V telluride exhibit a 2 × 1 structure, very similar to the one observed in multilayers of chromium ditelluride. The comparison of LEED and STM studies of MBE grown ML and multilayer samples is shown in Figure 6.

The multilayer structure was initially interpreted as a 1T' structure because this would give a similar 2 × 1 superstructure. 32,52 However, no 1T' structure is known for VTe₂, and the known 1T'' of bulk VTe₂, which should exhibit a 3×1 superstructure, was never observed in MBE grown multilayer films. The similarities of the STM images of the vanadium telluride films with those of Cr-telluride multilayers suggest that an intercalation compound is also obtained for V tellurides, i.e., TMDCs with ¹/₂ ML of excess V intercalated in between the layers. This is reasonable considering that the V₃Te₄ intercalation compound is a prominent phase in the vanadium telluride phase diagram, 53,54 and our DFT calculations summarized in Table 1 also show that the V₃Te₄-like bilayer structure has the lowest total energy among the intercalation compounds. DFT calculations of the crystal structure of a bilayer with $\frac{1}{2}$ layer intercalation show similar buckling in the TMDC layer as for Cr telluride, and consequently, the simulated STM images also show corrugation that is in close agreement with the experimental data as shown in Figure 6f. Thus, the STM characterization of the multilayer films is consistent with the formation of an intercalation compound.

Further support for a transition from VTe₂ in the ML to an intercalation compound comes from a compositional analysis by XPS (note that no such analysis has been done for chromium telluride because of the overlap of the core-levels for Cr-2p and Te-3d prevents such an analysis in chromium telluride system). In this analysis, we compare the change of the Te/V peak intensities as a function of film thickness, without attempting an accurate compositional determination because of poorly defined transmission function of our energy analyzer. Thus, we only study the relative change in the composition. Figure 7 shows XPS spectra for V-2p and Te-3d

with a Shirley background and the fitted peaks. Importantly, the Te/V atomic ratio decreases with increasing film thickness. This is consistent with vanadium being intercalated in between TMDC layers, given rise to higher V concentration with increasing film thickness compared to pure TMDC MLs. However, the increase in XPS measurements appears to be somewhat smaller than anticipated for an intercalation compound. This may be related to background subtraction in the V-spectrum, which is generally challenging because of the presence of shakeup satellite in the V-2p spectrum. 55,56 In addition to a change in the Te/V peak intensity ratio, we also observe a small shift of the V-2p (\sim -0.3 eV) and Te-3d (\sim 0.4 eV) peaks to lower and higher binding energies, respectively, as a function of film thickness. The shift of the Te-3d core-level binding energy to higher binding energy for multilayer films compared to the ML may have different contribution. For a pure charge transfer (or chemical shift), one may expect a shift in the opposite direction as the presence of more V-cations in the compound should lead to more negative tellurium. However, core-level shifts can have different origins. Surrounding of the Te-sites with more cations, as is the case for intercalation compounds, changes the electrostatic potential at the Te-site, which would result in a shift to higher binding energy^{57,58} as observed in our data and thus this is consistent with the formation of a self-intercalation compound. Finally, we also conducted a cross-sectional STEM analysis of multilayer samples, see Supporting Information, Figure S4. Both the in-plane lattice constant, as well as the interlayer separation measured in STEM, are consistent with an intercalation compound.

Thus, we conclude that chromium telluride and vanadium telluride grow similarly in our MBE study. The main difference appears in the ML regime, where the ML TMDC forms readily for VTe₂ while chromium telluride requires low growth temperatures to stabilize it as a TMDC. This difference may be understood in the relative stability of the layered TMDC phases, where VTe₂ is known to be a stable compound, while CrTe₂ is only metastable in bulk. In this respect, TiTe₂, whose TMDC phase has an even lower formation energy than that of VTe₂, is an interesting case to be investigated and is discussed next.

Titanium Telluride. Ultrathin TiTe, has attracted interest because it has been demonstrated that the ML exhibits a CDW, while no CDW is known for bulk TiTe₂. The CDW transition temperature of the ML was determined from angleresolved photoemission spectroscopy (ARPES) studies to 92 K, while no CDW was observed for the bi- and multilayer samples in this study. However, a recent study on multilayers grown by MBE on InAs substrates observed a 2 × 2 sample reconstruction that persisted to room temperature (the highest temperature investigated).²⁹ This structure was explained as a room temperature CDW, but no transition temperature to a normal phase could be given. Precise determination of the lattice constants by synchrotron XRD, in this study, revealed that the lattice constant slightly varied from the expected values of TiTe2. This led the authors to conclude that the film was strained through substrate effects, and it was proposed that this strain induces a phonon instability that causes the CDW.⁶⁰ We point out, however, that the measured lattice constants are very close to the intercalation compound Ti₅Te₈ or Ti₂Te₃. which would also exhibit a 2×2 or 2×1 superstructure in the basal planes with respect to the TiTe₂ hexagonal plane (see Figure 1). Thus, the intercalation of excess Ti should be

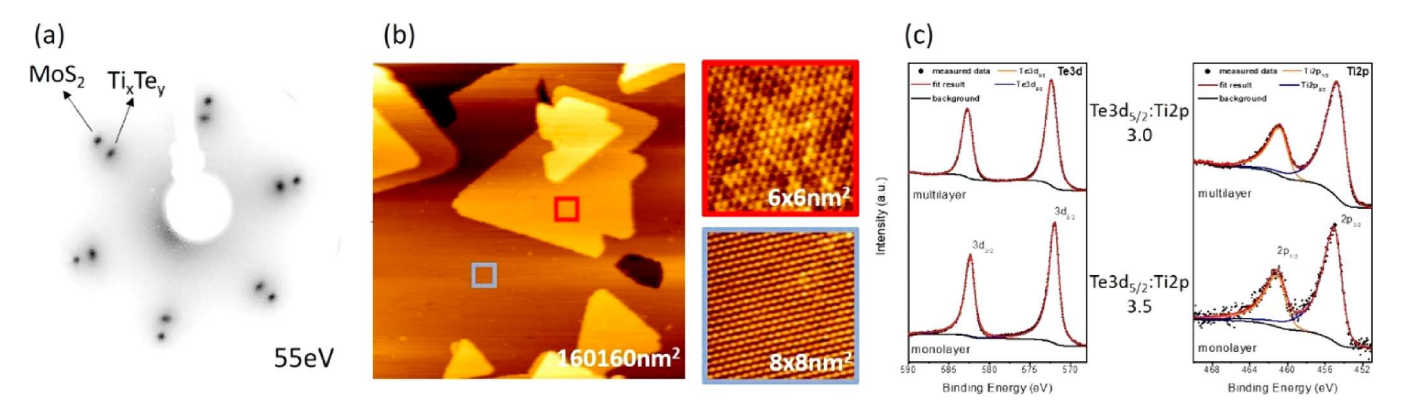


Figure 8. Ti_xTe_y multilayer sample. (a) LEED pattern of the film grown on MoS_2 substrate showing a 1×1 pattern, indicative of a lack of long-range periodicity for multilayer. (b) Large scale STM image showing complete ML with bilayer and trilayer island. High resolution STM of a ML and bilayer region showing a 1×1 structure in both regions. Bilayer regions show contrast variations but no long-range periodicity other than 1×1 structure. STM images were taken on a film grown on the HOPG substrate. (c) Layer-dependent XPS spectra of Ti 2p and Te 3d used to compare the change of the Te/Ti peak intensities as a function of film thickness for Ti_xTe_y on HOPG samples. STM imaging conditions (sample bias, tunneling current): (b) large scale 1.2 V, 0.7 nA, red square -10 mV, 0.7 nA, blue square -0.1 V, 0.7 nA.

considered as a possible alternative explanation for the observed 2 \times 2 structure rather than a CDW instability. In the specific case of titanium telluride, $TiTe_2$, Ti_3Te_4 , Ti_2Te_3 , and Ti_5Te_8 are all known phases 61 and thus should be considered as potential phases that can be obtained during MBE growth.

Here, we investigate the growth of titanium telluride by MBE on van der Waals substrates to elucidate the possibility for the formation of intercalation compounds. We find that ML growth on MoS₂ or HOPG van der Waals substrates results in 1T-TiTe₂ films, which is confirmed by both STM as well as LEED, which only exhibits 1 × 1 structure, as shown in Figure 8. LT-STM studies at 20 K of the ML exhibits a 2 × 2 superstructure (see Supporting Information, Figure SS), which is consistent with the reported CDW for ML TiTe₂. ¹⁷ In contrast to the well-ordered ML sample, second layer islands exhibit contrast variations on the atomic scale with some shortrange order, *e.g.*, a dominance of "brighter" atoms aligning in a row, but no long-range periodicity is observed, as shown in the insets of Figure 8b.

These defect structures persist in multilayer films. A lack of long-range periodicity is also observed in LEED for multilayer films grown on MoS_2 substrates that continue to exhibit only 1×1 diffraction spots. Does this mean there are no intercalated atoms in $TiTe_2$? As STM indicates in multilayers, there are clear corrugations that are on a short scale a 2×1 or 2×2 structure but lack long-range periodicity, and this may explain the lack of superstructure in LEED. Furthermore, the corrugation of these short-range corrugations is much weaker, and detailed bias dependent STM studies, shown in Figure 9c, indicate that these modulations are best observed at low bias voltages.

DFT calculations of a bilayer $TiTe_2$ with $^1/_2$ a ML intercalated Ti is shown in Figure 9a. It is apparent from the calculated structure that the intercalant induced buckling of the surface is much reduced compared to the same compositions for V- and Cr- tellurides. Supporting Information, Table S1, summarizes the calculated buckling in the surface layer for the M_xTe_y compounds. This weak buckling also gives rise to very small contrast differences in simulated STM images, shown in Figure 9b. Consequently, the experimental STM data are consistent with the presence of intercalated Ti-atoms in multilayer Ti telluride. Self-intercalation in multilayers is also

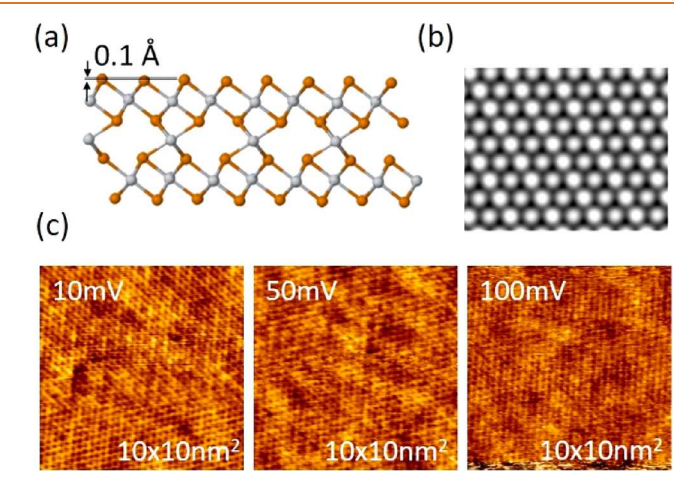


Figure 9. Structural characterization of self-intercalated TiTe₂. (a) DFT calculation of a bilayer TiTe₂ with $^{1}/_{2}$ a metal layer intercalated. The intercalant induced corrugation of the surface layer is much reduced compared to equivalent structures of V- or Cr- tellurides. This also causes only very weak contrast in simulated STM images shown in (b). Experimental bias dependence STM images for Ti_xTe_y multilayer sample grown on MoS_2 are shown in (c). Some structural modulations are seen at low bias voltages that are consistent with local ordering in a 2 \times 1 structure, but no long-range order is observed. STM image information (sample bias, tunneling current): (c) 10 mV, 0.9 nA; 50 mV, 0.9 nA; 100 mV, 0.9 nA.

evident by comparing XPS intensity ratios for mono- and multilayer films, shown in Figure 8c. Increasing the film thickness from ML to multilayer, the Te-3d/Ti-2p ratio decreased by about 30%, indicating a higher Ti concentration in multilayer films.

CONCLUSIONS

The early transition metal (Ti, V, Cr) tellurides are known for their many diverse quantum phenomena. Advances in tuning properties of van der Waals materials by reducing their number of layers and/or combining them into artificial van der Waals heterostructures also increased the interest in growing such ML and multilayer samples by molecular beam epitaxy (MBE). However, in addition to these dichalcogenides, a series of related compounds exist that share the dichalcogenide layer

structure but have additional transition metals in between these layers. These additional transition metals are periodically ordered and covalently bound to the dichalcogenide layers. These compounds are structurally very similar to the dichalcogenides and thus are challenging to discern from the dichalcogenides for ultrathin films. Here we showed that ML synthesis of 1T-TMDC could be achieved for all three early transition metal ditellurides by MBE, including for CrTe2, a compound that is only metastable in its bulk form. For multilayer growth, intercalation of transition metals in between the TMDC layers is observed in all three early transition metal tellurides studied here. For Cr- and V- tellurides, structures consistent with M3Te4 are found, while for Ti-telluride, the intercalants may only have local ordering. It should be pointed out that the compositions obtained in MBE may be different from those in other growth methods, and for example, vapor phase transport growth has reported the synthesis of multilayer 1T-VTe₂ platelets. 62,63 Generally, the structural similarities between TMDCs and some of the intercalation compounds can easily lead to misinterpretation of ultrathin films grown by MBE. While the unintentional formation of these intercalationlike compounds can lead to wrong data interpretation, a control of the composition of these materials can be used to synthesize variations of van der Waals materials, e.g., bilayer TMDCs with a single intercalated transition metal layer. We demonstrated that these intercalation compounds can be grown by van der Waals epitaxy on dissimilar van der Waals substrates, which indicates their potential for the synthesis as van der Waals heterostructures. Similarly, the growth of layered materials has been demonstrated on intercalation compound substrates (MBE grown Cr₂Te₃).⁴² Moreover, intercalation compounds, like V_3Se_4 , have been incorporated in a bulk van der Waals materials.⁶⁴ These studies indicate that few-layer intercalation compounds, terminated by TMDC layers, are an extension of van der Waals materials and can be useful "building-blocks" for MBE-grown van der Waals heterostructures.

METHODS

Experiment. The first row, early transition metal tellurides $(V_x Te_y)$ Ti_xTe_y, and Cr_xTe_y) have been grown by codeposition of the transition metal and tellurium in an ultrahigh vacuum MBE chamber on van der Waals substrates. In this study, we use HOPG-or MoS₂ substrates. The substrates are freshly cleaved in air and subsequently outgassed in vacuum at 300 °C for at least 2 h before growth. MoS₂ substrates are synthetically grown commercial single crystalline samples. V, Ti, and Cr are evaporated from a mini e-beam evaporator, while Te is codeposited from a K-cell. The Te flux exceeds the transition metal flux by a factor of ~10. The improvement of the ML CrTe2 film structure was observed after increasing Te:Cr flux ratio to a factor of ~20. Intercalated compounds of Cr₃Te₄, V₃Te₄, and Ti₃Te₄ were grown at the substrate temperature between 300 and 350 °C. ML CrTe₂ was stabilized for substrate temperatures of about 200 °C. The growth rate of all the TMDs studied here was adjusted to ~1 ML/15 min. The grown samples were transferred in situ from the growth chamber to a surface analysis chamber. The analysis chamber is equipped with LEED, room temperature STM, and XPS. XPS studies are performed with Al K α radiation from a nonmonochromatized dual anode X-ray source. The photoemitted electrons were detected with a Scienta R3000 hemispherical analyzer. Electrochemically etched tungsten tips were used for STM studies using an Omicron STM-1. Additional LT-STM studies were performed on ML TiTe₂ using an RHK Pan style closed-cycle STM cooled to ~20 K. For these studies, the samples were transferred in a vacuum suitcase from the growth chamber to the LT STM, without exposure to air.

STEM studies were conducted at the High Magnetic Field Laboratory in Tallahassee. For transfer, the samples were capped with a \sim 20 nm thick tellurium layer. A focus ion beam (FIB) was used to cut a thin lamella into the samples for cross-sectional analysis.

Computation. All the calculations were performed within density functional theory (DFT) as implemented in the Vienna *Ab Initio* Simulation Package (VASP) code $^{65-68}$ with Projector augmented wave pseudopotentials 69,70 and PBE 71 (GGA) functional. For the sampling of the Brillouin zone, a dense $30 \times 30 \times 1$ grid was used, while the plane wave energy cutoff was set to 500 eV. All the structures were optimized until the forces exerted on atoms were smaller than 10^{-5} eV/Å. STM images were simulated using Tersoff—Hamann method, 45 based on partial charge densities calculated by VASP. In the case of pristine bilayers, the van der Waals D3 correction method of Grimme et al. 72 with Becke — Jonson damping was applied. 73

The AIMD simulations were conducted using the OpenMX numerical code⁷⁴ which implements Nosé—Hoover molecular dynamics. The AIMD simulation of VASP calculations, the GGA PBE parametrization of XC part of the DFT Hamiltonian was used. For all the cases, the MD simulation lasted for 2 ps at temperatures of $T=500~\mathrm{K}$ and $T=600~\mathrm{K}$.

ASSOCIATED CONTENT

Supporting Information

The Supporting Information is available free of charge at https://pubs.acs.org/doi/10.1021/acsnano.0c02712.

Description of uncertainty estimate for lattice constants in STEM images; simulated STM images and respective structures of different intercalation compounds for $M_X Te_Y$ with M=Cr, V, Ti, STM and LEED for postgrowth annealing study for the evolution of $Cr Te_2 ML$ after annealing at 300 °C; *ab initio* molecular dynamics (AIMD) calculations for excess Cr on mono and bilayer $Cr Te_2$ (also AIMD movies of annealing processes are available); cross-section STEM image of $V_X Te_Y$; and LT STM at 20 K of ML $Ti Te_2$ (PDF)

AIMD movie of *ab initio* molecular dynamics simulations of the stability $CrTe_2$ -films with excess Cr atoms during annealing: $ML\ CrTe_2$ with $^1/_2\ ML$ excess Cr in between the ML and a MoS_2 substrate (Figure 5a) (MP4)

AIMD movie of *ab initio* molecular dynamics simulations of the stability $CrTe_2$ -films with excess Cr atoms during annealing: bilayer $CrTe_2$ with $^1/_2$ ML Cr intercalated in between the two layers (Figure 5b) (MP4)

AIMD movie simulation of CrTe₂ with excess Cr on top for monolayer, Figure S3s (MP4)

AIMD movie simulation of CrTe₂ with excess Cr on top for bilayer CrTe₂, Figure S3b (MP4)

AUTHOR INFORMATION

Corresponding Author

Matthias Batzill — Department of Physics, University of South Florida, Tampa, Florida 33620, United States; ⊚ orcid.org/ 0000-0001-8984-8427; Email: mbatzill@usf.edu

Authors

Kinga Lasek — Department of Physics, University of South Florida, Tampa, Florida 33620, United States

Paula Mariel Coelho – Department of Physics, University of South Florida, Tampa, Florida 33620, United States

Krzysztof Zberecki – Faculty of Physics, Warsaw University of Technology, 00-662 Warsaw, Poland

Yan Xin — National High Magnetic Field Laboratory, Florida State University, Tallahassee, Florida 32310, United States Sadhu K. Kolekar — Department of Physics, University of South Florida, Tampa, Florida 33620, United States Lingfeng Li — Department of Physics, University of South

Jingfeng Li – Department of Physics, University of South Florida, Tampa, Florida 33620, United States

Complete contact information is available at: https://pubs.acs.org/10.1021/acsnano.0c02712

Notes

The authors declare no competing financial interest.

ACKNOWLEDGMENTS

Financial support from the National Science Foundation under award NSF-DMR 1701390 is acknowledged. TEM work was performed at the National High Magnetic Field Laboratory, which is supported by National Science Foundation Cooperative Agreement no. DMR-1644779 and the State of Florida. Numerical calculations were supported in part by PL-Grid Infrastructure.

REFERENCES

- (1) Qiao, Q.; Zhou, S.; Tao, J.; Zheng, J.-C.; Wu, L.; Ciocys, S. T.; Iavarone, M.; Srolovitz, D. J.; Karapetrov, G.; Zhu, Y. Anisotropic Charge Density Wave in Layered 1T—TiSe₂. *Phys. Rev. Mater.* **2017**, *1*, No. 054002.
- (2) Mottas, M.-L.; Jaouen, T.; Hildebrand, B.; Rumo, M.; Vanini, F.; Razzoli, E.; Giannini, E.; Barreteau, C.; Bowler, D. R.; Monney, C.; Beck, H.; Aebi, P. Semimetal-To-Semiconductor Transition and Charge-Density-Wave Suppression in $1T-TiSe_{2-x}S_x$ Single Crystals. *Phys. Rev. B: Condens. Matter Mater. Phys.* **2019**, 99, 155103.
- (3) Rossnagel, K. On the Charge Density Waves in Select Layered Transition-Metal DichalcogenideS. *J. Phys.: Condens. Matter* **2011**, 23, 213001.
- (4) Cercellier, H.; Monney, C.; Clerc, F.; Battaglia, C.; Despont, L.; Garnier, M. G.; Beck, H.; Aebi, P.; Patthey, L.; Berger, H.; Forró, L. Evidence for an Excitonic Insulator Phase in 1T–TiSe₂. *Phys. Rev. Lett.* **2007**, *99*, 146403.
- (5) Eaglesham, D. J.; Withers, R. L.; Bird, D. M. Charge-Density-Wave Transitions in 1T-VSe₂. J. Phys. C: Solid State Phys. 1986, 19, 359–367.
- (6) Yan, C.; Gong, C.; Wangyang, P.; Chu, J.; Hu, K.; Li, C.; Wang, X.; Du, X.; Zhai, T.; Li, Y.; Xiong, J. 2D Group IVB Transition Metal Dichalcogenides. *Adv. Funct. Mater.* **2018**, 28, 1803305.
- (7) Morosan, E.; Zandbergen, H. W.; Dennis, B. S.; Bos, J. W. G.; Onose, Y.; Klimczuk, Y.; Ramirez, A. P.; Ong, N. P.; Cava, R. J. Superconductivity in Cu_xTiSe₂. *Nat. Phys.* **2006**, *2*, 544–550.
- (8) Kusmartseva, A. F.; Sipos, B.; Berger, H.; Forro, L.; Tutis, E. Pressure Induced Superconductivity in Pristine1T-TiSe₂. *Phys. Rev. Lett.* **2009**, *103*, 236401.
- (9) Joe, Y. I.; Chen, X. M.; Ghaemi, P.; Finkelstein, K. D.; de la Peña, G. A.; Gan, Y.; Lee, J. C. T.; Yuan, S.; Geck, J.; MacDougall, H. J.; Chiang, T. C.; Cooper, S. L.; Fradkin, E.; Abbamonte, P. Emergence of Charge Density Wave Domain Walls above the Superconducting Dome in 1T-TiSe₂. *Nat. Phys.* **2014**, *10*, 421–425.
- (10) Dutta, U.; Malavi, P. S.; Sahoo, S.; Joseph, B.; Karmakar, S. Pressure-Induced Superconductivity in Semimetallic 1T—TiTe₂ and its Persistence upon Decompression. *Phys. Rev. B: Condens. Matter Mater. Phys.* **2018**, *97*, No. 060503(R).
- (11) Freitas, D. C.; Weht, R.; Sulpice, A.; Remenyi, G.; Strobel, P.; Gay, F.; Marcus, J.; Nunez-Regueiro, M. Ferromagnetism in Layered Metastable 1T-CrTe₂. *J. Phys.: Condens. Matter* **2015**, *27*, 176002.
- (12) Bonilla, M.; Kolekar, S.; Ma, Y.; Coy Diaz, H.; Kalappattil, V.; Das, R.; Eggers, T.; Gutierrez, H. R.; Phan, M.-H.; Batzill, M. Strong Room-Temperature Ferromagnetism in VSe₂ Monolayers on van der Waals Substrates. *Nat. Nanotechnol.* **2018**, *13*, 289–293.

- (13) Coelho, P. M.; Nguyen Cong, K. N.; Bonilla, M.; Kolekar, S.; Phan, M.-H.; Avila, J.; Asensio, M. C.; Oleynik, I. I.; Batzill, M. Charge Density Wave State Suppresses Ferromagnetic Ordering in VSe, Monolayers. *J. Phys. Chem. C* **2019**, *123*, 14089–14096.
- (14) Sugawara, K.; Nakata, Y.; Shimizu, R.; Han, P.; Hitosugi, T.; Sato, T.; Takahashi, T. Unconventional Charge-Density-Wave Transition in Monolayer 1T-TiSe₂. ACS Nano **2016**, 10, 1341–1345.
- (15) Kolekar, S.; Bonilla, M.; Ma, Y.; Diaz, H. C.; Batzill, M. Layerand Substrate-Dependent Charge Density Wave Criticality in 1T—TiSe₃. 2D Mater. **2018**, 5, No. 015006.
- (16) Duong, D. L.; Ryu, G.; Hoyer, A.; Lin, C.; Burghard, M.; Kern, K. Raman Characterization of the Charge Density Wave Phase of 1T-TiSe2: From Bulk to Atomically Thin Layers. *ACS Nano* **2017**, *11*, 1034–1040.
- (17) Chen, P.; Pai, W. W.; Chan, A.; Takayama, C.-Z.; Xu, A.; Karn, S.; Hasegawa, M. Y.; Chou, S.-K.; Mo, A.-V.; Fedorov, T.-C.; Chiang. Emergence of Charge Density Waves and a Pseudogap in Single-Layer TiTe₂. *Nat. Commun.* **2017**, *8*, 516.
- (18) Duvjir, G.; Choi, B. K.; Jang, I.; Ulstrup, S.; Kang, S.; Ly, T. T.; Kim, S.; Choi, Y. H.; Jozwiak, C.; Bostwick, A.; Rotenberg, E.; Park, J.-G.; Sankar, R.; Kim, K.-S.; Kim, J.; Chang, Y. J. Emergence of a Metal—Insulator Transition and High-Temperature Charge-Density Waves in VSe₂ at the Monolayer Limit. *Nano Lett.* **2018**, *18*, 5432—5438.
- (19) Feng, J.; Biswas, D.; Rajan, A.; Watson, M. D.; Mazzola, F.; Clark, O. J.; Underwood, K.; Marković, I.; McLaren, M.; Hunter, A.; Burn, D. M.; Duffy, L. B.; Barua, S.; Balakrishnan, G.; Bertran, F.; Le Fèvre, P.; Kim, T. K.; van der Laan, G.; Hesjedal, T.; Wahl, P.; King, P. D. C. Electronic Structure and Enhanced Charge-Density Wave Order of Monolayer VSe₂. *Nano Lett.* **2018**, *18*, 4493–4499.
- (20) Chen, P.; Pai, W. W.; Chan, Y.-H.; Madhavan, V.; Chou, M. Y.; Mo, S.-K.; Fedorov, A.-V.; Chiang, T.-C Unique Gap Structure and Symmetry of the Charge Density Wave in Single-Layer VSe₂. *Phys. Rev. Lett.* **2018**, *121*, 196402.
- (21) Wong, P. K. J.; Zhang, W.; Bussolotti, F.; Yin, X.; Herng, T. S.; Zhang, L.; Huang, Y. L.; Vinai, G.; Krishnamurthi, S.; Bukhvalov, D. W.; Zheng, Y. J.; Chua, R.; N'Diaye, A. T.; Morton, S. A.; Yang, C.-Y.; Yang, K.-H. O.; Torelli, P.; Chen, W.; Goh, K. E. J.; Ding, J.; et al. Evidence of Spin Frustration in a Vanadium Diselenide Monolayer Magnet. *Adv. Mater.* **2019**, *31*, 1901185.
- (22) Kolekar, S.; Bonilla, M.; Diaz, H. C.; Hashimoto, M.; Lu, D.; Batzill, M. Controlling the Charge Density Wave Transition in Monolayer TiSe₂: Substrate and Doping Effects. *Adv. Quantum Technol.* **2018**, *1*, 1800070.
- (23) Rajan, A.; Underwood, K.; Mazzola, F.; King, P. D. C. Morphology Control of Epitaxial Monolayer Transition Metal Dichalcogenides. *Phys. Rev. Mater.* **2020**, *4*, No. 014003.
- (24) Sugawara, K.; Nakata, Y.; Fujii, K.; Nakayama, K.; Souma, S.; Takahashi, T.; Sato, T. Monolayer VTe₂: Incommensurate Fermi Surface Nesting and Suppression of Charge Density WaveS. *Phys. Rev. B: Condens. Matter Mater. Phys.* **2019**, *99*, 241404.
- (25) Wang, Y.; Ren, J.; Li, j.; Wang, Y.; Peng, H.; Yu, P.; Duan, W.; Zhou, S. Evidence of Charge Density Wave with Anisotropic Gap in a Monolayer VTe₂ Film. *Phys. Rev. B: Condens. Matter Mater. Phys.* **2019**, *100*, 241404.
- (26) Wong, P. K. J.; Zhang, W.; Zhou, J.; Bussolotti, F.; Yin, X.; Zhang, L.; N'Diaye, A. T.; Morton, S. A.; Chen, W.; Goh, K. E. J.; de Jong, M. P.; Feng, Y. P.; Wee, A. T. S. Metallic 1T Phase, 3d¹ Electronic Configuration and Charge Density Wave Order in Molecular Beam Epitaxy Grown Monolayer Vanadium Ditelluride. *ACS Nano* 2019, 13, 12894–12900.
- (27) Miao, G.; Xue, S.; Li, B.; Lin, Z.; Liu, B.; Zhu, X.; Wang, W.; Guo, J. Real-Space Investigation of the Charge Density Wave in VTe₂ Monolayer with Broken Rotational and Mirror Symmetries. *Phys. Rev. B: Condens. Matter Mater. Phys.* **2020**, *101*, No. 035407.
- (28) Won, D.; Kiem, D. H.; Cho, H.; Kim, D.; Kim, Y.; Jeong, M. Y.; Seo, C.; Kim, J.; Park, J.-G.; Han, M. J.; Yang, H.; Cho, S. Polymorphic Spin, Charge, and Lattice Waves in Vanadium Ditelluride. *Adv. Mater.* **2020**, 32, 1906578.

- (29) Fragkos, S.; Sant, R.; Alvarez, C.; Bosak, A.; Tsipas, P.; Tsoutsou, D.; Okuno, H.; Renaud, G.; Dimoulas, A. Room Temperature Commensurate Charge Density Wave in Epitaxial Strained TiTe₂ Multilayer Films. *Adv. Mater. Interfaces* **2019**, *6*, 1801850.
- (30) Duvjir, G.; Choi, B. K.; Ly, T. T.; Lam, N. H.; Chun, S.-H.; Jang, K.; Soon, A.; Chang, Y. J.; Kim, J. Novel Polymorphic Phase of Two-Dimensional VSe₂: the 1T' Structure and its Lattice Dynamics. *Nanoscale* **2019**, *11*, 20096–20101.
- (31) Chen, G.; Howard, S. T.; Maghirang, A. B., III; Cong, K. N.; Cai, K.; Ganguli, S. C.; Sweich, W.; Morosan, E.; Oleynik, I. I.; Chuang, F.-C.; Lin, H.; Madhavan, V. Correlating Structural, Electronic, and Magnetic Properties of Epitaxial VSe₂ Thin Films. arXiv:1912.12798v2. 2020, https://arxiv.org/abs/1912.12798v2 (accessed 2020-05-27).
- (32) Coelho, P. M.; Lasek, K.; Nguyen Cong, K.; Li, J.; Niu, W.; Liu, W.; Oleynik, I. I.; Batzill, M. Monolayer Modification of VTe₂ and its Charge Density Wave. *J. Phys. Chem. Lett.* **2019**, *10*, 4987–4993.
- (33) Ueda, Y.; Ohtani, T. Mechanochemical Synthesis, Vacancy-Ordered Structures and Low-Dimensional Properties of Transition Metal Chalcogenides. In *Handbook of Solid State Chemistry*, 1st ed.; Dronskowski, R., Kikkawa, S., Stein, A. Wiley-VCH: Weinheim, 2017; Vol. 1, pp 383–434.
- (34) Hayashi, A.; Imada, K.; Inoue, K.; Ueda, Y.; Kosuge, K. Phase Diagram of $(M'_xM_{1-x})_3Se_4$ (0 < x < 1) (M, M' = 3D-Transition Metal). *Bull. Inst. Chem. Res., Kyoto Univ.* **1986**, *64*, 186–206.
- (35) Ipser, H.; Komarek, K. I.; Klepp, K. Transition Metal-Chalcogen Systems VIII: The Cr-Te Phase Diagram. *J. Less-Common Met.* 1983, 92, 265–282.
- (36) Dijkstra, J.; Weitering, H. H.; van Bruggen, C. F.; Haas, C.; de Groot, R. A. Band-Structure Calculations, and Magnetic and Transport Properties of Ferromagnetic Chromium Tellurides (CrTe, Cr3Te4, Cr,Te,). *J. Phys.: Condens. Matter* **1989**, *1*, 9141–9161.
- (37) Yamaguchi, M.; Hashimoto, T. Magnetic Properties of Cr₃Te₄ in Ferromagnetic Region. *J. Phys. Soc. Jpn.* **1972**, *32*, 635–638.
- (38) Wang, F.; Du, J.; Sun, F.; Sabirianov, R. F.; Al-Aqtash, N.; Sengupta, D.; Zeng, H.; Xu, X. Ferromagnetic Cr₂Te₃ Nanorods with Ultrahigh Coercivity. *Nanoscale* **2018**, *10*, 11028–11033.
- (39) Wen, Y.; Liu, Z.; Zhang, Y.; Xia, C.; Zhai, B.; Zhang, X.; Zhai, G.; Shen, C.; He, P.; Cheng, R.; Yin, L.; Yao, Y.; Sendeku, M. G.; Wang, Z.; Ye, X.; Liu, C.; Jiang, C.; Shan, C.; Long, Y.; He, J. Tunable Room-Temperature Ferromagnetism in Two-Dimensional Cr₂Te₃. *Nano Lett.* **2020**, *20*, 3130–3139.
- (40) Freitas, D. C.; Weht, R.; Sulpice, A.; Remenyi, G.; Strobel, P.; Gay, F.; Marcus, J.; Nunez-Regueiro, M. Ferromagnetism in Layered Metastable 1T-CrTe₂. *J. Phys.: Condens. Matter* **2015**, *27*, 176002.
- (41) van Bruggen, C. F.; Haange, R. J.; Wiegers, G. A.; de Boer, D. K. G. CrSe₂, a New Layered Dichalcogenide. *Physica B+C* **1980**, *99*, 166–172.
- (42) Roy, A.; Guchhait, S.; Dey, R.; Pramanik, T.; Hsieh, C.-C.; Rai, A.; Banerjee, S. K. Perpendicular Magnetic Anisotropy and Spin Glass-Like Behavior in Molecular Beam Epitaxy Grown Chromium Telluride Thin Films. *ACS Nano* **2015**, *9*, 3772–3779.
- (43) Burn, D. M.; Duffy, L. B.; Fujita, R.; Zhang, S. L.; Figueroa, A. I.; Herrero-Martin, J.; van der Laan, G.; Hesjedal, T. Cr₂Te₃ Thin Films for Integration in Magnetic Topological Insulator Heterostructures. *Sci. Rep.* **2019**, *9*, 10793.
- (44) Li, H.; Wang, L.; Chen, J.; Yu, T.; Zhou, L.; Qiu, Y.; He, H.; Ye, F.; Sou, I. K.; Wang, G. Molecular Beam Epitaxy Grown Cr₂Te₃ Thin Films with Tunable Curie Temperatures for Spintronic Devices. *ACS Appl. Nano Mater.* **2019**, *2*, 6809–6817.
- (45) Hui, L.; Lim, S. T.; Bi, J. F.; Teo, K. L. Investigation on the Antiferromagnetic Component in the Intrinsic Exchange Bias in Structurally Single Phase Cr₂Te₃ Thin Film. *J. Appl. Phys.* **2012**, *111*, No. 07D719.
- (46) Tersoff, J.; Hamann, D. R. Theory of the Scanning Tunneling Microscope. *Phys. Rev. B: Condens. Matter Mater. Phys.* **1985**, 31, 805–813.

- (47) Springer Materials Database. https://materials.springer.com/(accessed 2020-05-27).
- (48) Bronsema, K. D.; Bus, G. W.; Wiegers, G. A. The Crystal Structure of Vanadium Ditelluride, V_{1+x} Te₂. J. Solid State Chem. **1984**, 53, 415–421.
- (49) Chen, C.; Kim, H.-S.; Admasu, A. S.; Cheong, S.-W.; Haule, K.; Vanderbilt, D.; Wu, W. Trimer Bonding States on the Surface of the Transition-Metal Dichalcogenide TaTe₂. *Phys. Rev. B: Condens. Matter Mater. Phys.* **2018**, 98, 195423.
- (50) Chen, H.; Li, Z.; Fan, X.; Guo, L.; Chen, X. Quantum Linear Magnetoresistance in NbTe₂. *Solid State Commun.* **2018**, 275, 16–20.
- (51) Sörgel, T.; Nuss, J.; Wedig, U.; Kremer, R. K.; Jansen, M. A New Low Temperature Modification of TaTe₂—Comparison to the Room Temperature and the Hypothetical 1T-TaTe₂ Modification. *Mater. Res. Bull.* **2006**, *41*, 987–1000.
- (52) Dai, T.; Kang, S.; Ma, X.; Dang, S.; Li, H.; Ruan, Z.; Zhou, W.; Hu, P.; Li, S.; Wu, S. Multiple Transitions of Charge Density Wave Order in Epitaxial Few-Layered 1T'-VTe₂ Films. *J. Phys. Chem. C* **2019**, *123*, 18711–18716.
- (53) Terzieff, P.; Ipser, H.; Wachtel, E. Transition Metal-Chalcogen Systems IX: The Vanadium-Tellurium System Phase Diagram and Magnetic Properties. *J. Less-Common Met.* **1986**, *119*, 1–12.
- (54) Ohtani, T.; Nishihara, H.; Koga, K. Structure Refinement and Physical Properties of the V₃Te₄ Phase. *Solid State Commun.* **1989**, *71*, 1179–1184.
- (55) Vernon, G. A.; Stucky, G.; Carlson, T. A. Comprehensive Study of Satellite Structure in the Photoelectron Spectra of Transition Metal Compounds. *Inorg. Chem.* **1976**, *15*, 278–284.
- (56) Silversmit, G.; Depla, D.; Poelman, H.; Marin, G. B.; De Gryse, R. Determination of the V2p XPS Binding Energies for Different Vanadium Oxidation States (V⁵⁺ to V⁰⁺). J. Electron Spectrosc. Relat. Phenom. **2004**, 135, 167–175.
- (57) Pueyo Bellafont, N.; Bagus, P. S.; Illas, F. Prediction of Core Level Binding Energies in Density Functional Theory: Rigorous Definition of Initial and Final State Contributions and Implications on the Physical Meaning of Kohn-Sham Energies. *J. Chem. Phys.* **2015**, 142, 214102.
- (58) Bagus, P. S.; Illas, F.; Pacchioni, G.; Parmigiani, F. Mechanisms Responsible for Chemical Shifts of Core-Level Binding Energies and their Relationship to Chemical Bonding. *J. Electron Spectrosc. Relat. Phenom.* 1999, 100, 215–236.
- (59) Kirklin, S.; Saal, J. E.; Meredig, B.; Thompson, A.; Doak, J. W.; Aykol, M.; Rühl, S.; Wolverton, C. The Open Quantum Materials Database (OQMD): Assessing the Accuracy of DFT Formation Energies. *npj Comput. Mater.* **2015**, *1*, 15010.
- (60) Guster, B.; Robles, R.; Pruneda, M.; Canadell, E.; Ordejón, P. 2 × 2 Charge Density Wave in Single-Layer TiTe₂. 2D Mater. **2019**, 6, No. 015027.
- (61) Cordes, H.; Schmid-Fetzer, R. Phase Equilibria in the Ti-Te System. *J. Alloys Compd.* **1995**, 216, 197–206.
- (62) Li, J.; Zhao, B.; Chen, P.; Wu, R.; Li, B.; Xia, Q.; Guo, G.; Luo, J.; Zang, K.; Zhang, Z.; Ma, H.; Sun, G.; Duan, X.; Duan, X. Synthesis of Ultrathin Metallic MTe₂ (M = V, Nb, Ta) Single-Crystalline Nanoplates. *Adv. Mater.* **2018**, *30*, 1801043.
- (63) Liu, H.; Xue, Y.; Shi, J.-A.; Guzman, R. A.; Zhang, P.; Zhou, Z.; He, Y.; Bian, C.; Wu, L.; Ma, R.; Chen, J.; Yan, J.; Yang, H.; Shen, C.-M.; Zhou, W.; Bao, L.; Gao, H.-J. Observation of the Kondo Effect in Multilayer Single-Crystalline VTe₂ Nanoplates. *Nano Lett.* **2019**, *19*, 8572–8580.
- (64) Gunning, N. S.; Dankwort, T.; Falmbigl, M.; Ross, U.; Mitchson, G.; Hamann, D. M.; Lotnyk, A.; Kienle, L.; Johnson, D. C. Expanding the Concept of van der Waals Heterostructures to Interwoven 3D Structures. *Chem. Mater.* **2017**, *29*, 8292–8298.
- (65) Kresse, G.; Hafner, J. Ab Initio Molecular Dynamics for Liquid Metals. Phys. Rev. B: Condens. Matter Mater. Phys. 1993, 47, 558–561.
- (66) Kresse, G.; Hafner, J. Ab Initio Molecular-Dynamics Simulation of the Liquid-Metal—Amorphous-Semiconductor Transition in Germanium. Phys. Rev. B: Condens. Matter Mater. Phys. 1994, 49, 14251–14269.

- (67) Kresse, G.; Furthmüller, J. Efficiency of *Ab-Initio* Total Energy Calculations for Metals and Semiconductors Using a Plane-Wave Basis Set. *Comput. Mater. Sci.* **1996**, *6*, 15–50.
- (68) Kresse, G.; Furthmüller, J. Efficient Iterative Schemes for *Ab Initio* Total-Energy Calculations Using a Plane-Wave Basis Set. *Phys. Rev. B: Condens. Matter Mater. Phys.* **1996**, *54*, 11169–11186.
- (69) Blöchl, P. E. Projector Augmented-Wave Method. Phys. Rev. B: Condens. Matter Mater. Phys. 1994, 50, 17953.
- (70) Kresse, G.; Joubert, D. From Ultrasoft Pseudopotentials to the Projector Augmented-Wave Method. *Phys. Rev. B: Condens. Matter Mater. Phys.* **1999**, *59*, 1758–1775.
- (71) Perdew, J. P.; Burke, K.; Ernzerhof, M. Generalized Gradient Approximation Made Simple. *Phys. Rev. Lett.* **1996**, *77*, 3865–3868.
- (72) Grimme, S.; Antony, J.; Ehrlich, S.; Krieg, S. A Consistent and Accurate *Ab Initio* Parametrization of Density Functional Dispersion Correction (DFT-D) for the 94 Elements H-Pu. *J. Chem. Phys.* **2010**, 132, 154104.
- (73) Grimme, S.; Ehrlich, S.; Goerigk, L. Effect of the Damping Function in Dispersion Corrected Density Functional Theory. *J. Comput. Chem.* **2011**, 32, 1456–1465.
- (74) Ozaki, T. Variationally Optimized Atomic Orbitals for Large-Scale Electronic Structures. *Phys. Rev. B: Condens. Matter Mater. Phys.* **2003**, *67*, 155108.
- (75) Nosé, S. A Unified Formulation of the Constant Temperature Molecular Dynamics Methods. *J. Chem. Phys.* **1984**, *81*, 511–519.
- (76) Nosé, S. A Molecular Dynamics Method for Simulations in the Canonical Ensemble. *Mol. Phys.* **1984**, *52*, 255–268.
- (77) Hoover, G. H. Canonical Dynamics: Equilibrium Phase-Space Distributions. *Phys. Rev. A: At., Mol., Opt. Phys.* **1985**, *31*, 1695–1697.